



CrossMark
click for updates

Cite this: *RSC Adv.*, 2016, 6, 88531

Zinc and linkage effects of novel porphyrin-containing polyimides on resistor memory behaviors†

Chia-Liang Tsai,^{‡a} Kamani Sudhir K Reddy,^{‡b} Chen-Yu Yeh,^{*b} Chin-Li Wang,^c Ching-Yao Lin,^{*c} Hung-Ju Yen,^a Ming-Chi Tsai^a and Guey-Sheng Liou^{*a}

A new class of porphyrin-containing polyimides, ZnPor-*s*-DSDA, ZnPor-*t*-DSDA, Por-*s*-DSDA and Por-*t*-DSDA, were synthesized from porphyrin-containing diamines and 3,3',4,4'-diphenylsulfone tetracarboxylic dianhydride for resistor-type memory applications. The effect of the linkage and zinc metal was investigated by electrochemistry, molecular simulations, and memory behaviors. The memory devices with different retention times derived from polymers ZnPor-*s*-DSDA (WORM, >3 h) and ZnPor-*t*-DSDA (DRAM, 30 s) demonstrated the importance of the linkage effect, and the insulation property of polyimides Por-*s*-DSDA and Por-*t*-DSDA also implies a crucial memory behavior by metal chelation.

Received 26th July 2016
Accepted 30th August 2016

DOI: 10.1039/c6ra18986e

www.rsc.org/advances

Introduction

Polymers have become remarkable synthetic materials in these last few decades and have been applied in novel fields, including solar cells,¹ organic thin film transistors (OTFTs),² organic light-emitting diodes (OLEDs),³ electrochromic devices,⁴ and memory devices.⁵ After the first polymeric memory device was demonstrated by Sliva *et al.* in 1970,⁶ polymer-based memory devices have attracted immense attention. They have been studied for the development of the next generation of memory device applications because of their low-cost, three-dimensional stacked structure, organo-process ability, and large area fabrication capability.⁷ Moreover, there are numerous types of polymer materials that have been investigated for memory devices, which generally includes conjugated polymers featuring donor-acceptor (D-A) capabilities,⁸ non-conjugated polymers bearing side-chain electroactive chromophores,⁹ functionalized polyimides (PIs),¹⁰ and polymer hybrids.¹¹ According to the rich structural flexibility of polymeric materials, different types of memory behaviors have been demonstrated, including volatile devices, such as static random access memory (SRAM) and dynamic

random access memory (DRAM), and nonvolatile devices such as write-once-read-many times (WORM) and rewritable memory (Flash). Among these polymer systems, functional PI was chosen for a polymeric memory application due to the excellent combination of advantages such as outstanding thermal properties, chemical resistance, and good mechanical properties. In 2006, Kang *et al.* published the first PI-based resistor-type memory device, showing a programmable DRAM behavior.¹² A resistive memory device stores data by bi-stable states (high and low conductivities), “1 (ON)” and “0 (OFF)”. Furthermore, the working mechanism of resistor-type memory devices has been studied and divided into charge transfer (CT), filamentary conduction, and space charge trapping. CT is defined as the partial electronic D-A charge transfers. Thus, D-A system based memory devices can easily induce CT that results by applying suitable external voltage.¹³

Notably, porphyrin-containing materials were widely used in organic devices, including solar cells,¹⁴ LEDs,¹⁵ and TFTs.¹⁶ In particular, porphyrin derivatives have been demonstrated as good π -bridge moieties due to their high degrees of conjugation, electron-rich structures, and excellent extinction coefficients, which further make porphyrin-based materials a great candidate for solar-cell applications.

In this study, we design three new D-A porphyrin-based PIs, Por-*t*-DSDA, ZnPor-*s*-DSDA, and Por-*s*-DSDA, for resistor-type memory applications (Fig. 1), which are also compared with ZnPor-*t*-DSDA.¹⁷ In addition, the works published by our lab^{18a,b} report tunable memory behaviors with various donors and the same acceptor, 3,3',4,4'-diphenylsulfone tetracarboxylic dianhydride (DSDA), to compare their electron-donating abilities. By further choosing the suitable linkage between the electron donor and acceptor moieties of high performance polymers,

^aInstitute of Polymer Science and Engineering, National Taiwan University, 1 Roosevelt Road, 4th Sec., Taipei 10617, Taiwan. E-mail: gслиou@ntu.edu.tw

^bDepartment of Chemistry and Research Center for Sustainable Energy and Nanotechnology, National Chung Hsing University, Taichung 402, Taiwan. E-mail: cyyeh@dragon.nchu.edu.tw

^cDepartment of Applied Chemistry, National Chi Nan University, Puli, Nantou 54561, Taiwan. E-mail: cyl@ncnu.edu.tw

† Electronic supplementary information (ESI) available: Experimental section. Table: basic properties of polyimides. Figure: basic properties of monomers and polyimides. See DOI: 10.1039/c6ra18986e

‡ These authors contributed equally.



Fig. 1 Chemical structure of porphyrin-based PIs and memory device.

tunable memory properties (from insulator to different retention time SRAM) can also be achieved.^{18c} Therefore, this D–A PI system consists of electron donor macrocyclic porphyrin derivatives and an excellent acceptor DSDA.¹⁸ The memory behavior of Zn porphyrin-containing PIs (**ZnPor-*t*-DSDA** and **ZnPor-*s*-DSDA**) exhibit DRAM (30 s) and WORM (>3 h), respectively, according to different linkages between donor (Zn-porphyrin diamines) and acceptor (DSDA) moieties. However, based on the experimental results, free base porphyrin-containing PIs (**Por-*t*-DSDA** and **Por-*s*-DSDA**) did not show any memory behavior under an applied voltage, indicating that zinc is necessary to induce CT by an external electric field.

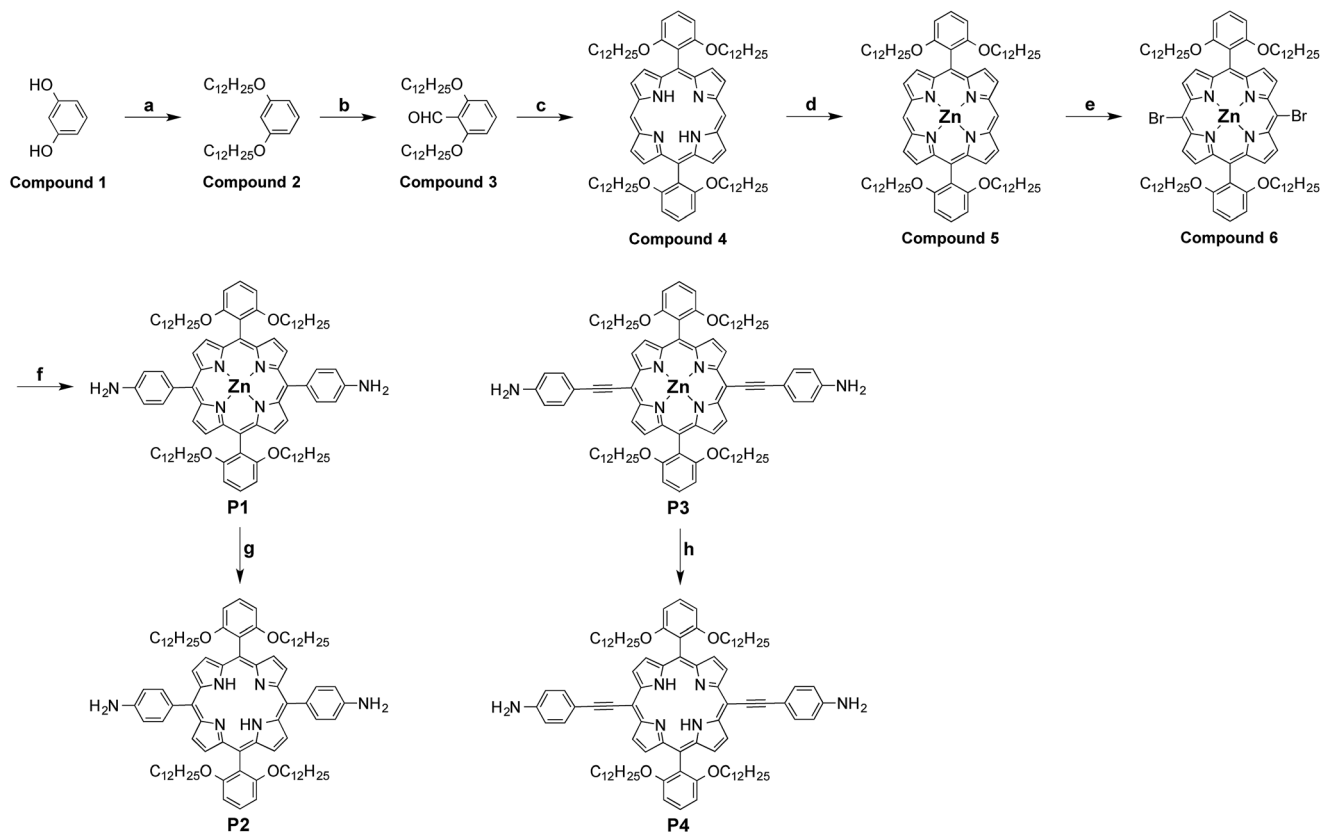
Results and discussion

Monomer synthesis

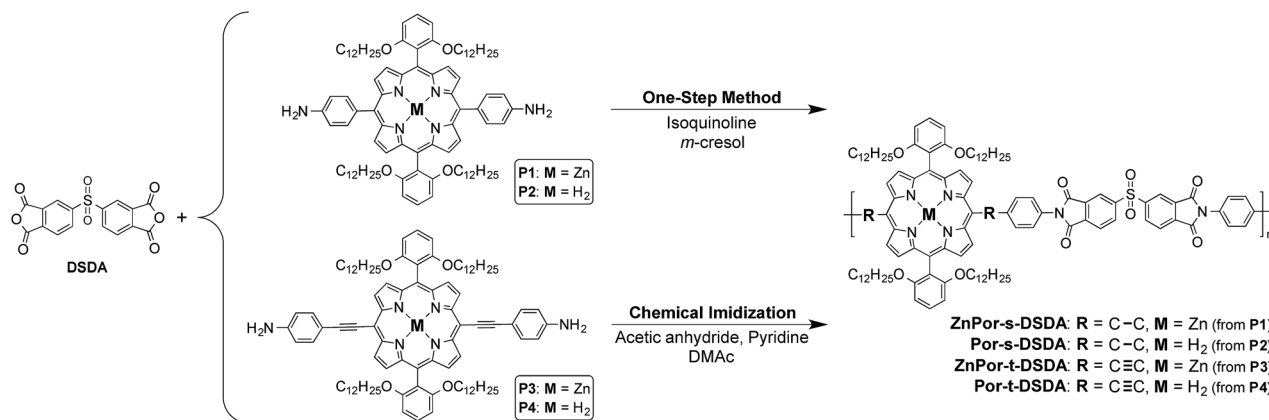
The synthetic procedure for diamines **P1–P4** is summarized in Scheme 1 and was based on previous strategies.¹⁹ The significant intermediate compound **6** was prepared with a yield of >26% from the Lewis acid (trifluoroacetic acid) catalyzed condensation of compound **3** and dipyrromethane followed by zinc-metallation and dibromination. Diamine **P1** was prepared by Pd-catalyzed Sonogashira coupling, which was then used to prepare **P2** by demetallation. Similarly, diamine **P4** was also synthesized by demetallation of **P3**. ¹H NMR, ¹³C NMR, elemental analysis, and MALDI-TOF MS were utilized to characterize the structure of these new compounds. The bulky alkoxyphenyl long chains were incorporated at the meso-positions to prevent aggregation that can further facilitate the organo-solubility of the prepared porphyrin-based polyimides.

Basic properties of porphyrin-containing PIs

Three novel porphyrin-containing PIs were prepared by the reaction of four different porphyrin diamines (**P1–P4**) and DSDA *via* a conventional polycondensation reaction, as shown in Scheme 2. A porphyrin moiety was introduced as a donor of PIs in this study because of its planar, electron-rich, highly



Scheme 1 Synthetic procedure for the formation of diamines **P1–P4**. Conditions: (a) DMSO, 1-bromododecane, KOH, room temperature, 12 h, (b) 1.6 M *n*-BuLi, DMF, (c) dipyrromethane, TFA, CH₂Cl₂, (d) Zn(OAc)₂·4H₂O, CH₂Cl₂, CH₃OH, (e) NBS, CH₂Cl₂, pyridine, –5 °C to room temperature, (f) Pd(PPh₃)₄, 4-(4,4,5,5-tetramethyl-1,3,2-dioxaborolan-2-yl)aniline, Na₂CO_{3(aq)}, toluene, 100 °C for 5 h, (g) 16% HCl, CH₂Cl₂, room temperature, (h) 12 M HCl, CH₂Cl₂, CH₃OH, room temperature, Na₂CO_{3(aq)}.



Scheme 2 Synthesis and structures of the porphyrin containing polyimides.

conjugated, and easily tunable chemical structure. The inherent viscosity and GPC data of the PIs are listed in Table S1,[†] and the solubility properties examined at 5 wt% are summarized in Table S2.[†] The results exhibited an excellent organo-solubility of these porphyrin-containing PIs due to the wrapping of the long alkoxy chains and the polarity of DSDA. Thus, good solubility renders these PIs as outstanding memory materials for a solvent-casting process. The thermal behaviors of the porphyrin-containing PIs were investigated by TGA and TMA, and the diagrams shown in Fig. S1[†] revealed good thermal properties with negligible weight loss up to 330 °C and a glass-transition temperature (T_g) in the range of 132–176 °C (Table S3[†]).

Optical and electrochemical properties

The UV spectra of the porphyrin-containing PIs are depicted in Fig. S2,[†] and the energy gap (E_g) of the prepared polymers was calculated by the onset wavelength. Electrochemistry was tested by cyclic voltammetry (CV) *via* casting the PIs onto ITO-coated glass substrates as working electrodes with 0.1 M tetrabutylammonium perchlorate (TBAP) containing dehydrate acetonitrile (CH₃CN) as an electrolyte solution under a nitrogen atmosphere. The CV shown in Fig. 2 displayed the onset oxidation potentials of the PIs (**ZnPor-t-DSDA**, **Por-t-DSDA**, **ZnPor-s-DSDA**, and **Por-s-DSDA**) to be 0.79, 0.99, 0.75, and 1.00 V, which are related to the highest occupied molecular orbital (HOMO) of 5.23, 5.43, 5.19, and 5.44 eV, respectively, (based on the ferrocene/ferrocenium redox couple, which is 4.8 eV below the vacuum level with $E_{\text{onset}} = 0.36$ V). The results summarized in Table 1 reveal that the HOMO energy levels of the Zn-porphyrin-containing PIs (**ZnPor-t-DSDA** and **ZnPor-s-DSDA**) are higher than those of the corresponding Zn-free PIs, implying that the Zn-porphyrin has a higher electron-donating capability.

Memory device characteristics

The memory properties of PIs were characterized by the current–voltage (I – V) diagrams of an ITO-coated glass/PI/Al or Au sandwiched device (as shown in Fig. 1). The PI film that

served as an active layer was spin-coated between ITO and Al. A standard thickness of ~50 nm was employed to exclude the thickness effect. The I – V curves of **ZnPor-s-DSDA** depicted in Fig. 3(a) and (b) show the nonvolatile bi-switching WORM memory property. With the first negative and positive scan from 0 to –6 and 6 V, the device was initially in the OFF state with a current around $\sim 10^{-12}$ A, then increased sharply from the OFF state to $\sim 10^{-4}$ A (ON state) at threshold voltages of –4.2 V and 4.6 V, respectively.

The device derived from **ZnPor-s-DSDA** remained in the ON state in the succeeding negative and positive sweeps after turning the power off for a long period of time (>3 h), which is very different from the device derived from **ZnPor-t-DSDA** that displayed bi-switching DRAM behavior (retention time only 30 s) in our previous study.¹⁷

Furthermore, the long-term operation at the ON and OFF states of the ITO/**ZnPor-s-DSDA**/Al device with a continuously applied voltage of –1 V was tested and shown in Fig. 4. There is negligible degradation in current at both the ON and OFF states

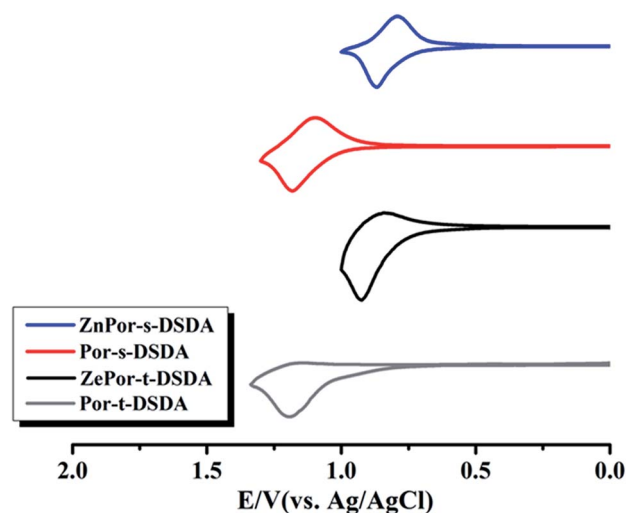


Fig. 2 CVs of PI films on an ITO-coated glass in 0.1 M TBAP/CH₃CN at a scan rate of 50 mV s⁻¹.

Table 1 Oxidation potentials and energy levels of PIs

Polymer	Oxidation E_{onset}^a (V)	E_g^b (eV)	HOMO ^c (eV)	LUMO ^d (eV)
ZnPor- <i>t</i> -DSDA	0.79	1.78	5.23	3.45
ZnPor- <i>s</i> -DSDA	0.75	1.98	5.19	3.21
Por- <i>t</i> -DSDA	0.99	1.72	5.43	3.71
Por- <i>s</i> -DSDA	1.00	1.86	5.44	3.58

^a From CVs vs. Ag/AgCl in CH₃CN. ^b The data are calculated from the onset wavelength by the equation: $E_g = 1240/\lambda_{\text{onset}}$ (energy gap between HOMO and LUMO). ^c The HOMO energy levels were calculated from CV and were referenced to ferrocene (4.8 eV; $E_{\text{onset}} = 0.36$ V). ^d LUMO energy levels were calculated by the optical method from E_g and HOMO.

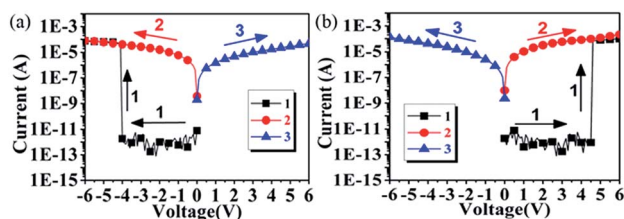


Fig. 3 I - V diagrams of the ITO/ZnPor-*s*-DSDA/Al memory devices with the first scan performed (a) negatively and (b) positively.

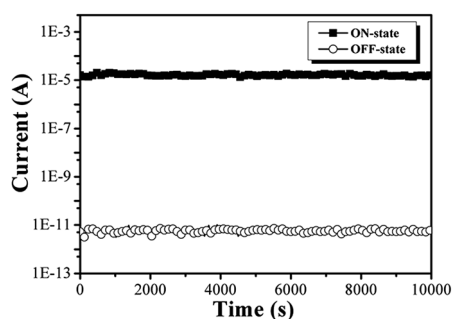


Fig. 4 Long-term operation at the ON and OFF states of the ITO/ZnPor-*s*-DSDA/Al device with a continuously applied voltage of -1 V for ON and OFF states.

after 10^4 s under the readout test, indicating the excellent stability of the memory device. The devices prepared from **Por-*s*-DSDA** and **Por-*t*-DSDA** exhibited no memory properties with the corresponding voltage sweeps shown in Fig. 5(a) and (b), respectively.

Simulation of switching mechanism

To obtain deep insight into the memory performance of porphyrin-based PIs, a molecular simulation of the basic unit was performed at the B3LYP/LanL2DZ level of theory using Gaussian 09. The calculated HOMO and LUMO of the prepared PIs are illustrated in Fig. 6(a). For the electron distribution, the HOMO and LUMO are mainly located at the donor porphyrin moieties and acceptor DSDA, respectively. As the applied external electric field reached the threshold voltage, some electrons localizing at the HOMO transit to the LUMOs, forming a CT formation (ON state). Transit of electrons to the LUMO5 (**ZnPor-*s*-DSDA**) and the LUMO3 (**ZnPor-*t*-DSDA**) is a more likely

possibility according to the highest overlap of the electron distribution between the HOMO and LUMO5/3. Moreover, other LUMOs in between would possibly accept the electrons excited from the HOMO. Thus, the conductive CT complexes were formed by several pathways, including the LUMO5/3 through LUMOs in between, then to the LUMO or direct excitation from the HOMO to the LUMO due to intra-/inter-molecular CT. Moreover, the generated electron holes can delocalize to porphyrin moieties, performing an open channel for charge carriers (holes), and therefore switched the device to the ON state. Nevertheless, **Por-*s*-DSDA** and **Por-*t*-DSDA**, displaying similar simulation results as the zinc containing ones, revealed no memory properties, confirming the crucial effect of zinc on the formation of conductive channels.

According to the simulation results shown in Fig. 6(b), the different conformation due to the linkage between the porphyrin unit and the phenyl ring of **ZnPor-*s*-DSDA** (single bond) and **ZnPor-*t*-DSDA** (triple bond) resulted in 65.5° and 0.4° , respectively. The induced electrons localize at the DSDA moiety by applying an electric field, and the non-coplanar (65.5°) conformational structure of **ZnPor-*s*-DSDA** becomes a barrier for CT back from the DSDA to the porphyrin moiety, resulting in a much longer retention time (>3 h) than of **ZnPor-*t*-DSDA** (30 s). The linkage and non-coplanar effects on memory properties have also been investigated and were demonstrated in our previous reports.²⁰

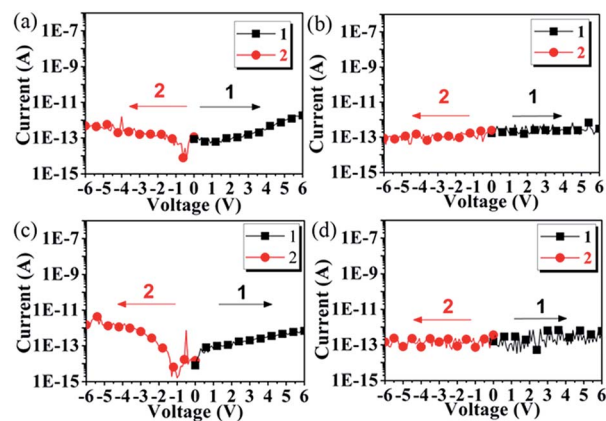


Fig. 5 I - V diagrams of the ITO/(a) Por-*s*-DSDA, (b) Por-*t*-DSDA/Al memory devices, and ITO/(c) Por-*s*-DSDA, (d) Por-*t*-DSDA/Au memory devices.

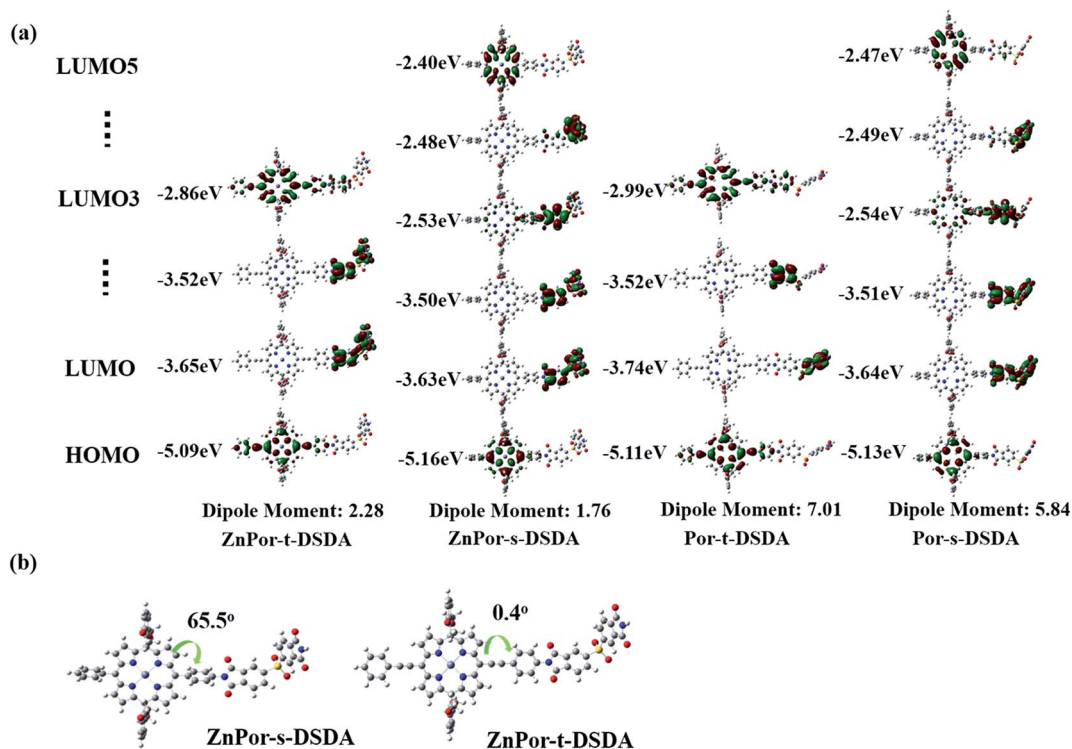


Fig. 6 (a) Molecular simulation of the corresponding energy levels and (b) twist angles of different linkages for the basic units of porphyrin-containing polyimides.

It is worth mentioning that the memory properties could be induced by both negative and positive sweeps in the porphyrin PIs with zinc. However, the corresponding PIs without zinc did not exhibit any memory behavior. In general, the injection of holes is from the ITO (-4.8 eV) to the HOMO of PI in the negative sweep because of the lower band gap between them, according to the proposed mechanism for PI memory devices. On the contrary, it is obviously difficult to induce a memory behavior when positively sweeping, as shown in Fig. 7(a). However, the devices derived from ITO/Por-s-DSDA and Por-t-DSDA/Al could not exhibit any memory properties even in a negative sweep, as illustrated in Fig. 5(a) and (b), indicating that the formation of the conductive channel or the injection of holes should be difficult for the PIs without zinc. Moreover, we also investigated the memory behavior by replacing an Al with an Au electrode referring to our previous studies²¹ in terms of the different work functions of the metal electrodes (Au 5.1 eV and Al 4.2 eV), and the memory property might be easily induced by a lower work function of the Au electrode. With this in mind, we fabricated the devices of ITO/Por-s-DSDA, Por-t-DSDA/Au, however, the devices still displayed no memory property in either negative nor positive sweeps, as shown in Fig. 5(c) and (d), respectively.

According to the experiment results, the occurrence of memory behaviors could be inferred from the effect of zinc. Fig. 7(b) depicts a schematic of the band diagram for the memory device of ITO/Zn-porphyrin-containing PI/Al. The work functions of Zn, ITO, and Al are very close (4.3, 4.8 and 4.2 eV, respectively). Thus, when an external electric field (negative or

positive) is applied to induce CT of the PIs, as shown in the molecular simulation, the generated holes will delocalize to the porphyrin moieties, thus resulting in an open channel for charge carrier migration. In addition, because zinc is chelated in the center of the porphyrin units, another possible route might be from ITO (negative sweep) or Al (positive sweep) through zinc to the porphyrin rings, resulting in the ON state due to an abrupt increase in current.

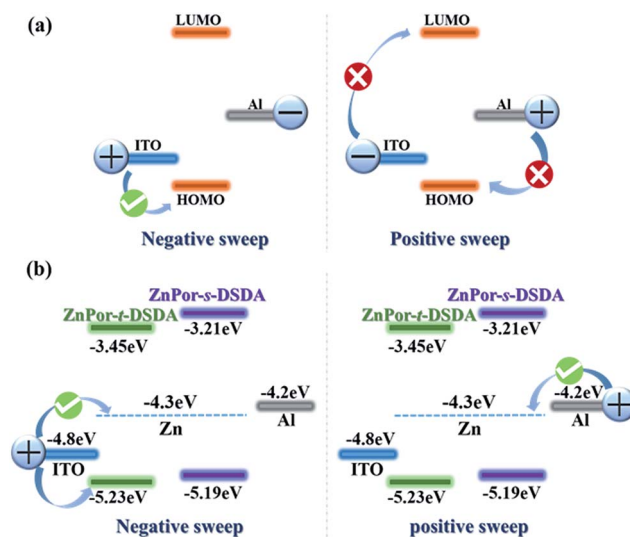


Fig. 7 (a) Band diagram for general polyimide memory devices and (b) ITO/zinc porphyrin-containing polyimide/Al.

Conclusions

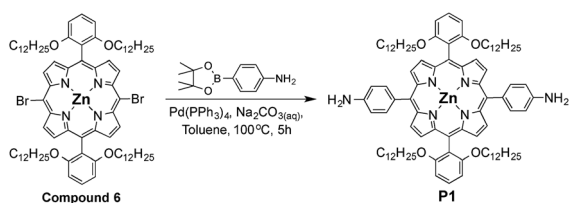
Three novel porphyrin-containing polyimides, **ZnPor-s-DSDA**, **Por-s-DSDA**, and **Por-t-DSDA**, were successfully prepared for memory device applications. **ZnPor-s-DSDA** and **ZnPor-t-DSDA** exhibit WORM (>3 h) and DRAM (30 s), respectively, ascribed to the linkage effect. The linkage resulting in a non-coplanar PI structure could increase the retention time effectively. The interesting effect of zinc on the memory behavior is noteworthy. Only devices derived from these Zn-containing PIs (**ZnPor-s-DSDA** and **ZnPor-t-DSDA**) displayed memory properties. The **Por-s-DSDA** and **Por-t-DSDA** based devices have no memory characteristics, demonstrating the significance of the presence of zinc, which is the trigger for memory properties. Further understanding about the working mechanism and the use of different metals (work function effect) of the metal-chelating porphyrin-containing polymers in memory applications is very important and in progress.

Experimental

Materials

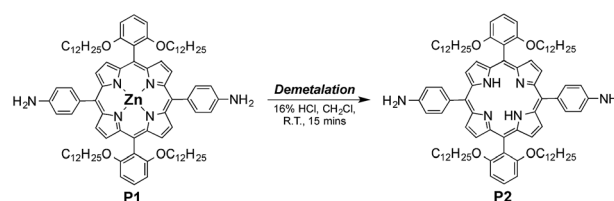
Air-sensitive materials were manipulated in a glove box (MBraun Unilab). In addition, air-sensitive solutions were processed with vacuum Schlenk lines. **P3** was synthesized according to our previous report.¹⁷ [5,15-Dibromo-10,20-bis(2,6-dioctoxyphenyl)porphinato]zinc(II) (compound **6**) was synthesized according to modified literature conditions¹⁹ and the detailed synthetic procedure and characterization of the precursors (compounds 2 to 6) are in the ESI.† Commercially available 3,3',4,4'-diphenylsulfone tetracarboxylic dianhydride (DSDA) was purchased from TCI and purified by sublimation. Tetrabutylammonium perchlorate (TBAP) (ACROS) was purified by recrystallization from ethyl acetate under a nitrogen atmosphere and then dried *in vacuo* prior to use. All other commercially available reagents were used as purchased.

Monomer synthesis

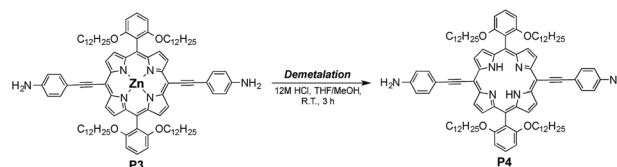


P1. To a solution, 2.5 g (1.73 mmol) of compound **6** in a 150 mL three-necked round bottom flask, 40 mL of toluene and 0.39 g (0.34 mmol) of tetrakis(triphenylphosphine)palladium were added and the mixture was stirred at room temperature for 30 min. To this solution, 5 mL of 2 M aqueous sodium carbonate was added, followed by 1.48 g (6.92 mmol) of 4-(4,4,5,5-tetramethyl-1,3,2-dioxaborolan-2-yl)aniline (Aldrich) in 10 mL of ethanol. The resulting mixture was heated at reflux until no remaining starting material was detected by thin layer chromatography (TLC). The reaction mixture was filtered through diatomaceous earth, washed

with ethyl acetate and subjected to column chromatography (silica gel) (dichloromethane/methanol = 9.8/0.2) followed by recrystallization to give 2.45 g of **P1** (97.22% in yield). ¹H NMR (400 MHz, CDCl₃): δ 8.87 (dd, *J* = 4.4 Hz, 4H), 8.83 (dd, *J* = 4.4 Hz, 4H), 7.91 (dd, *J* = 2 Hz, 4H), 7.67 (t, *J* = 8.4 Hz, 2H), 6.98 (d, *J* = 8.4 Hz, 2H), 6.76 (d, *J* = 8 Hz, 2H), 3.80 (t, *J* = 6.4 Hz, 8H), 3.11 (b, s NH, 4H), 1.53–0.365 (br, m, 92H). ¹³C NMR (100 MHz, CDCl₃): δ 160.35, 150.52, 150.33, 144.55, 135.53, 134.39, 131.70, 130.92, 129.59, 122.44, 122.44, 119.81, 114.97, 113.49, 112.93, 105.67, 68.93, 32.02, 31.08, 21.62, 29.47, 29.40, 29.21, 28.88, 28.81, 25.35, 22.82, 14.25. Elemental analysis for C₉₂H₁₁₀N₆O₄Zn: calcd C: 74.37, H: 11.26, N: 5.66; found C: 75.95, H: 9.16, N: 5.55. FAB-MS: *m/z* calcd for C₉₂H₁₂₆N₆O₄Zn 1442.9, found 1444.1 [M + 1]⁺.



P2. **P1** (1.0 g, 0.69 mmol) was dissolved in 100 mL of dichloromethane at room temperature with the addition of 16% HCl (25 mL) and stirred for 15 minutes. TLC showed the complete absence of compound **8**. The pH was adjusted to 7.5 with saturated NaHCO₃ and extracted with dichloromethane. The organic layer was dried over MgSO₄ followed by the removal of the solvent under reduced pressure. Recrystallization using dichloromethane/methanol gave 0.94 g of **P2** (98.9% yield). ¹H NMR (400 MHz, CDCl₃): δ 8.82 (d, *J* = 4.8 Hz, 4H), 8.77 (d, *J* = 4.4 Hz, 4H), 7.99 (d, *J* = 8.8 Hz, 4H), 7.69 (t, *J* = 8.8 Hz, 2H), 7.04 (d, *J* = 78.8 Hz, 4H), 6.99 (d, *J* = 8 Hz, 4H), 3.97 (b, NH₂, 4H), 3.81 (t, *J* = 6.4 Hz, 8H), 1.26–0.061 (br, m, 92H). –2.61 (s, 2H). ¹³C NMR (100 MHz, CDCl₃): δ 160.43, 145.84, 135.84, 133.40, 129.94, 129.75, 131.70, 121.52, 119.01, 113.57, 112.44, 105.52, 32.08, 29.71, 29.57, 29.49, 29.47, 29.30, 28.97, 28.84, 25.51, 22.87, 14.31, 1.26. Elemental analysis for C₉₂H₁₂₈N₆O₄: calcd C: 77.68, H: 11.91 N: 5.91; found C: 79.35, H: 9.88, N: 5.77. FAB-MS: *m/z* calcd for C₉₂H₁₂₈N₆O₄ 1381.0, found 1382.2 [M + 1]⁺.



P4. 200 mg (0.134 mmol) of **P3** (ref. 17) was dissolved in 80 mL of THF and 20 mL of methanol. After 10 mL of 12 M HCl(aq) was added, the mixture was stirred at room temperature for 3 h. The reaction was monitored by TLC until the disappearance of the starting material. Upon completion, 100 mL of Na₂CO₃(aq) was added slowly. The solvent was rotary evaporated and the residue was dissolved in dichloromethane again. After washed with aqueous NH₄Cl(aq) and dried over Na₂SO₄, the solvent was rotary evaporated. The residue was then purified by column chromatography (silica gel) using EA/hexanes = 1/3 as the eluent, followed by crystallization from dichloromethane/

methanol to give 137.2 mg of **P4** (dark green solid, 71.7% in yield). $^1\text{H-NMR}$ (300 MHz, CDCl_3): δ 9.53 (d, $J = 4.7$ Hz, 4H), 8.72 (d, $J = 4.6$ Hz, 4H), 7.78 (d, $J = 8.3$ Hz, 4H), 7.69 (t, $J = 8.4$ Hz, 2H), 6.98 (d, $J = 8.4$ Hz, 4H), 6.81 (d, $J = 8.3$ Hz, 4H), 3.92 (s, 4H), 3.83 (t, $J = 6.5$ Hz, 8H), 1.27–0.75 (m, overlapped, 58H), 0.75–0.27 (m, overlapped, 32H), -1.78 (s, 2H). Elemental anal for $\text{C}_{96}\text{H}_{128}\text{N}_6\text{O}_4 \cdot 0.5\text{H}_2\text{O}$: calcd C 80.12%, H 9.04%, N 5.84%; found: C 80.03%, H 8.96%, N 5.82%. MALDI-TOF: m/z calcd for $\text{C}_{96}\text{H}_{128}\text{N}_6\text{O}_4$ 1429.0; found 1429.8 $[\text{M} + \text{H}]^+$.

Polyimide synthesis

ZnPor-*t*-DSDA is provided as an example. The viscous poly(amic acid) can be obtained from a mixture of 0.224 g (0.15 mmol) of **P3** in 1.6 mL of *N,N*-dimethylacetamide (DMAc) and 0.054 g (0.15 mmol) of DSDA at room temperature for 16 hours. The as-prepared poly(amic acid) was then directly converted to PI **ZnPor-*t*-DSDA** via a chemical imidization method in the presence of acetic anhydride (0.6 mL) and pyridine (0.4 mL). After the reaction was processed at 120 °C for 4 h, the resulting PI solution was then poured into 300 mL of stirred methanol giving a fibrous precipitate, which was washed thoroughly with methanol and collected by filtration.

Acknowledgements

The authors gratefully acknowledge the Ministry of Science and Technology of Taiwan for financial support.

Notes and references

- (a) W. L. Ma, C. Y. Yang, X. Gong, K. Lee and A. J. Heeger, *Adv. Funct. Mater.*, 2005, **15**, 1617; (b) S. Gunes, H. Neugebauer and N. S. Sariciftci, *Chem. Rev.*, 2007, **107**, 1324; (c) Y. J. Cheng, S. H. Yang and C. S. Hsu, *Chem. Rev.*, 2009, **109**, 5868.
- (a) F. Garnier, R. Hajlaoui, A. Yassar and P. Srivastava, *Science*, 1994, **265**, 1684; (b) H. Yan, Z. H. Chen, Y. Zheng, C. Newman, J. R. Quinn, F. Dotz, M. Kastler and A. Facchetti, *Nature*, 2009, **457**, 679.
- (a) J. H. Burroughes, D. D. C. Bradley, A. R. Brown, R. N. Marks, K. Mackay, R. H. Friend, P. L. Burn and A. B. Holmes, *Nature*, 1990, **347**, 539; (b) R. H. Friend, R. W. Gymer, A. B. Holmes, J. H. Burroughes, R. N. Marks, C. Taliani, D. D. C. Bradley, D. A. Dos Santos, J. L. Bredas, M. Lögdlund and W. R. Salaneck, *Nature*, 1999, **397**, 121.
- (a) H.-J. Yen, C.-J. Chen and G.-S. Liou, *Adv. Funct. Mater.*, 2013, **23**, 5307; (b) Y. W. Chuang, H. J. Yen, J. H. Wu and G. S. Liou, *ACS Appl. Mater. Interfaces*, 2014, **6**, 3594; (c) J.-H. Wu and G.-S. Liou, *Adv. Funct. Mater.*, 2014, **24**, 6422.
- (a) J. H. Wu and G. S. Liou, *ACS Appl. Mater. Interfaces*, 2015, **7**, 15988; (b) H.-J. Yen, C.-J. Chen, J.-H. Wu and G.-S. Liou, *Polym. Chem.*, 2015, **6**, 7464.
- P. O. Sliva, G. Dir and C. Griffiths, *J. Non-Cryst. Solids*, 1970, **2**, 316.
- W. P. Lin, S. J. Liu, T. Gong, Q. Zhao and W. Huang, *Adv. Mater.*, 2014, **26**, 570.
- (a) H. C. Wu, C. L. Liu and W. C. Chen, *Polym. Chem.*, 2013, **4**, 5261; (b) H. J. Yen, H. Tsai, C. Y. Kuo, W. Nie, A. D. Mohite, G. Gupta, J. Wang, J. H. Wu, G. S. Liou and H. L. Wang, *J. Mater. Chem. C*, 2014, **2**, 4374; (c) W. Elsayw, M. Son, J. Jang, M. J. Kim, Y. Ji, T. W. Kim, H. C. Ko, A. Elbarbary, M. H. Ham and J. S. Lee, *ACS Macro Lett.*, 2015, **4**, 322.
- (a) S. L. Lim, Q. Ling, E. Y. H. Teo, C. X. Zhu, D. S. H. Chan, E. T. Kang and K. G. Neoh, *Chem. Mater.*, 2007, **19**, 5148; (b) S. G. Hahm, N. G. Kang, W. Kwon, K. Kim, Y. G. Ko, S. Ahn, B. G. Kang, T. Chang, J. S. Lee and M. Ree, *Adv. Mater.*, 2012, **24**, 1062; (c) S. J. Liu, P. Wang, Q. Zhao, H. Y. Yang, J. Wong, H. B. Sun, X. C. Dong, W. P. Lin and W. Huang, *Adv. Mater.*, 2012, **24**, 2901; (d) S. Miao, Y. Zhu, H. Zhuang, X. Xu, H. Li, R. Sun, N. Li, S. Ji and J. Lu, *J. Mater. Chem. C*, 2013, **1**, 2320.
- (a) L. C. Lin, H. J. Yen, C. J. Chen, C. L. Tsai and G. S. Liou, *Chem. Commun.*, 2014, **50**, 13917; (b) J. H. Wu, H. J. Yen, Y. C. Hu and G. S. Liou, *Chem. Commun.*, 2014, **50**, 4915.
- (a) A. D. Yu, C. L. Liu and W. C. Chen, *Chem. Commun.*, 2012, **48**, 383; (b) M. A. Khan, U. S. Bhansali, D. Cha and H. N. Alshareef, *Adv. Funct. Mater.*, 2013, **23**, 2145; (c) C. L. Tsai, C. J. Chen, P. H. Wang, J. J. Lin and G. S. Liou, *Polym. Chem.*, 2013, **4**, 4570; (d) C. J. Chen, J. H. Wu and G. S. Liou, *Chem. Commun.*, 2014, **50**, 4335.
- Q. D. Ling, F. C. Chang, Y. Song, C. X. Zhu, D. J. Liaw, D. S. Chan, E. T. Kang and K. G. Neoh, *J. Am. Chem. Soc.*, 2006, **128**, 8732.
- H.-J. Yen and G.-S. Liou, *Polym. J.*, 2016, **48**, 117.
- (a) A. Yella, H. W. Lee, H. N. Tsao, C. Yi, A. K. Chandiran, M. K. Nazeeruddin, E. W. Diau, C. Y. Yeh, S. M. Zakeeruddin and M. Gratzel, *Science*, 2011, **334**, 629; (b) C.-L. Wang, M. Zhang, Y.-H. Hsiao, C.-K. Tseng, C.-L. Liu, M. Xu, P. Wang and C.-Y. Lin, *Energy Environ. Sci.*, 2016, **9**, 200.
- (a) C. T. Chen, *Chem. Mater.*, 2004, **16**, 4389; (b) B. S. Li, J. Li, Y. Q. Fu and Z. S. Bo, *J. Am. Chem. Soc.*, 2004, **126**, 3430.
- (a) Y. Y. Noh, J. J. Kim, Y. Yoshida and K. Yase, *Adv. Mater.*, 2003, **15**, 699; (b) X. B. Huang, C. L. Zhu, S. M. Zhang, W. W. Li, Y. L. Guo, X. W. Zhan, Y. Q. Liu and Z. Z. Bo, *Macromolecules*, 2008, **41**, 6895.
- M.-C. Tsai, C.-L. Wang, C.-Y. Lin, C.-L. Tsai, H.-J. Yen, H.-C. You and G.-S. Liou, *Polym. Chem.*, 2016, **7**, 2780.
- (a) T.-T. Huang, C.-L. Tsai, S.-H. Hsiao and G.-S. Liou, *RSC Adv.*, 2016, **6**, 28815; (b) C.-J. Chen, H.-J. Yen, Y.-C. Hu and G.-S. Liou, *J. Mater. Chem. C*, 2013, **1**, 7623; (c) C. J. Chen, Y. C. Hu and G. S. Liou, *Chem. Commun.*, 2013, **49**, 2536; (d) Y.-H. Chou, H.-J. Yen, C.-L. Tsai, W.-Y. Lee, G.-S. Liou and W.-C. Chen, *J. Mater. Chem. C*, 2013, **1**, 3235.
- (a) C. Y. Lee and J. T. Hupp, *Langmuir*, 2010, **26**, 3760; (b) A. Yella, H. W. Lee, H. N. Tsao, C. Yi, A. K. Chandiran, M. K. Nazeeruddin, E. W. Diau, C. Y. Yeh, S. M. Zakeeruddin and M. Gratzel, *Science*, 2011, **334**, 629.
- (a) C.-J. Chen, Y.-C. Hu and G.-S. Liou, *Polym. Chem.*, 2013, **4**, 4162; (b) H.-J. Yen, J.-H. Chang, J.-H. Wu and G.-S. Liou, *Polym. Chem.*, 2015, **6**, 7758.
- C.-J. Chen, C.-L. Tsai and G.-S. Liou, *J. Mater. Chem. C*, 2014, **2**, 2842.